Korean J. Chem. Eng., **28**(9), 1814-1823 (2011)
DOI: 10.1007/s11814-011-0086-5

Wavelet texture analysis in process industries

J. Jay Liu*,† and Chonghun Han**

*Department of Chemical Engineering, Pukyong National University, Busan 608-737, Korea
**School of Chemical and Biological Engineering, Seoul National University, Seoul 151-742, Korea
(*Received 12 January 2011 • accepted 1 April 2011*)

Abstract−Wavelet texture analysis has been applied to solve many problems in process industries as well as in other industries. In solving problems from process industries however, its potentials have never been explored to the full extent yet. This is not only because techniques used in wavelet texture analysis are still unfamiliar to researchers and practitioners in process industries, but also because characteristics of the scenes displayed by the images in process industries are difficult to analyze: products and processes in process industries mostly have *stochastic* outside appearance. The purpose of this article is to give an overview of state-of-the-art methods in wavelet texture analysis through an illustrative example from process industries.

Key words: Image Texture Analysis, Process Industries, Stochastic Appearance, Wavelet Texture Analysis

INTRODUCTION

Since the advent of computers, image texture analysis has been studied for more than 60 years and one of the reasons for this can be the fact that there is no formal definition of texture. In fact, many researchers have described texture using various definitions because one can intuitively describe several image properties such as smoothness, coarseness, depth, regularity etc. with texture [1]. If the image can be represented as a two-dimensional surface on which each pixel is a square column, then the pixel intensity could be described by the height of each column in a three-dimensional histogram. As the adjacent pixel brightness variation increases, the surface of the three-dimensional histogram becomes less smooth. Texture can thus give a quantitative measure of the degree of surface roughness in an image. Alternatively, texture can be described as an attribute representing the spatial arrangement of the gray levels of the pixels in a region of a digital image [2]. Texture analysis has played an important role in many areas including medical imaging, remote sensing and inspection in manufacturing, and its tasks are mainly classification, segmentation, and synthesis [3-7].

Image texture analysis also has been applied to problems in process industries. On the contrary to typical manufacturing processes where images always provide a scene of objects with pre-defined size, shape, alignment, and so on, many processes in (chemical) process industries provide images where stochastic nature of the visual scene is dominant. In such processes, some hard-to-define outer appearance of products or processes is mostly major concern: color and morphology of froth in flotation processes [8,9], aesthetics of engineering-stone countertops [10], random visible pattern in injection-molded plastic panels [11], coating uniformity of medication tablets in an industrial coater [12], spatio-temporal variations of properties of polymer composite [13], quality control of paper formatoion [14] are just a few examples. In the example of surface roughness of rolled steel sheets [15], the quality of a steel sheet is related to the number and severity of pits on its surface. In the bad-quality steel sheets, the pits becomes deeper, start to be connected, and result in big and deep craters and valleys throughout the surface. There is no discontinuous class of surface quality in steel sheets and there also can be nearly an infinite number of patterns depending on the number and severity of pits. For this reason, *traditional* image texture analysis has had relatively little success in those problems until recently.

Just as the definitions of texture are various, the approaches for analyzing texture are also very diverse. In general, texture analysis methods can be divided into four categories [5,16]: (1) statistical methods that use pixel statistics, (2) structural methods that deal with the arrangement of image primitives, (3) model-based methods that construct a model of texture, and (4) transform-based methods that represent texture of an image in a transformed domain.

Among the four categories, transform-based methods are considered as the state of the art since they use various transforms to get spatial frequency information from an image, which is known to be closely related to texture. An important subclass of transform-based methods includes those based on space-frequency decompositions that decompose images into subimages with different spatial frequencies. The examples are the Gabor and Wavelet transforms. The Wavelet transform has emerged as a powerful method for texture analysis since wavelet transform has advantages over the Gabor transform in analyzing natural non-stationary signals [17]. Also, very efficient implementation of wavelet transform is possible using filter banks [17].

The aims of this paper are twofold: (1) provide a brief overview of image texture analysis approaches and (2) detail descriptions and illustrations of wavelet texture analysis by applying them to classification of industrial rolled steel sheets [15], which initiated many research works regarding texture analysis in Process Systems Engineering and Chemometrics communities. The focus of this paper will be on providing readers with not only detailed explanations

†To whom correspondence should be addressed.
E-mail: jayliu@pknu.ac.kr
‡An abridged version of this paper appears in the Proceeding of the ICCAS 2011 at KINTEX in Gyeonggi-do, Korea, October 2011.

about usage of wavelet texture analysis, but also the strengths and weakness of it. The rest of this paper is organized as follows. After a brief overview of image texture analysis methods, detail descriptions of wavelet texture analysis methods will be given in Section 2. Section 3 will give detailed illustration of wavelet texture analysis using the industrial case study. Conclusions are given in Section 4.

WAVELET TEXTURE ANALYSIS

1. A Brief Overview of Texture Analysis Methods

Statistical texture analysis techniques represent texture of regions in an image through the stochastic properties that govern the distributions and relationships between the grey levels of an image. In the study of visual perception of texture in terms of its statistical properties [18], the textures in grey-level images are discriminated spontaneously only if they differ in second order moments. Haralick proposed the use of a gray level co-occurrence matrix (GLCM) [19] which is related to second order statistics of the grayscale image histograms. This is probably the most frequently cited method for texture analysis and many variations of GLCM such as texture unit [20] and neighboring grey level dependence matrix (NGLDM) [21] have also been proposed. The GLCM method in general gives relatively good results in recent applications [13].

In contrast to statistical methods, structural texture analysis techniques [22] describe a texture as a hierarchy of spatial arrangements (*macrotextures*) of well-defined texture elements (*microtextures*) such as regularly spaced parallel lines [5]. The properties and placement rules of the texture elements define the image texture. Various structural texture analysis approaches have been proposed, ranging from using different shapes of structuring elements to conceiving real textures as distorted versions of ideal textures. Although the structural methods can provide a nice symbolic description of the texture, these methods appear to be limited in practicality since the abstract descriptions can be ill-defined for natural textures and thus they can only describe very regular textures [1,16].

Model-based texture analysis techniques construct an empirical image model that can be used to describe texture as well as to synthesize it. Usually the constructed models are based on a weighted average of the pixel intensities in its neighborhood. The estimated parameters of the image models capture the essential qualities of texture and thus they are used as textural feature descriptors. Markov random fields (MRF) [23] and fractal models [24] are popular examples of such model-based texture analysis methods. The high computational cost in the estimation of stochastic model parameters is the main problem of some model-based methods [16].

Transform-based texture analysis techniques represent an original image in a new space whose coordinates are closely related to texture (such as frequency, scale or size). It is well known that the success of these techniques strongly depends on the type of transform employed. It is reported that the performance of methods based on the Fourier transform is poor in practice, due to its lack of spatial localization [16]. The Gabor transform can provide better spatial localization but its practicality is limited because natural textures usually have multiple resolutions. The Wavelet transform is preferred to the Fourier or Gabor transforms since it provides varying spatial resolution and a wide range of selection of the wavelet functions, which allow it to represent textures at more suitable resolution and to adapt itself to a specific application.

2. Wavelet Texture Anlaysis

Among other methods for texture analysis, a wavelet-based method, which is often called wavelet texture analysis (WTA), is considered state of the art and it has shown better performance than others in many cases [5,6,25]. While the two-dimensional (2-D) Fast Fourier Transform (FFT) performs a frequency decomposition, the 2-D Gabor and wavelet transforms perform a space-frequency decomposition of an image. This is more suitable for texture analysis because there is strong psychophysical evidence that the human visual

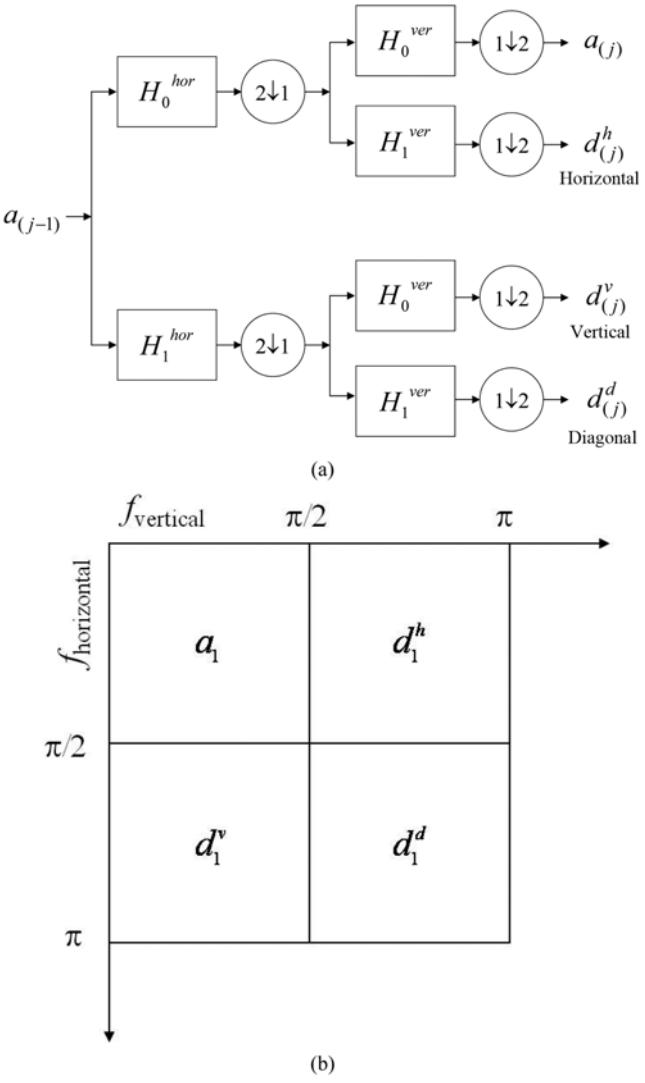

Fig. 1. A separable solution for two-dimensional DWT. (a) A separable two-dimensional filter bank at the *j*-th decomposition level consists of horizontal and vertical filtering of two-dimensional signals using low-pass and high-pass one-dimensional wavelet filters H_0 and H_1. 2↓1 and 1↓2 denote downsampling by 2 in horizontal and vertical directions respectively. (b) Division of the spatial frequency (f) spectrum of two-dimensional DWT at the first decomposition level. The subimage d_1^d captures high frequency ($\pi/2 \sim \pi$ in vertical and hirizontal directions) characteristics in the original image, while a_1 does low frequency ($0 \sim \pi/2$ in both directions) characteristics in the image.

system does multi-channel, space-frequency analysis [5]. The wavelet transform is preferred to the Gabor transform in the respect that the wavelet transform can maintain good space and frequency localization when (critically) sampled [17].

In achieving a 2-D discrete wavelet transform (DWT), there are two different solutions depending on the type of filters and the type of down-sampling lattices [17]. A separable solution is obtained easily if separable filters (Fig. 1(a)) are used. But the separable solution gives rectangular divisions of frequency spectrum (Fig. 1(b)) and strongly oriented coefficients (often called *subimages* because the wavelet coefficients for 2-D signals are also 2-D) in the horizontal, vertical, and diagonal directions (see Fig. 1).

A basic assumption for WTA is that a texture has its unique *signature* in the three-dimensional (3-D) scale-space consisting of spatial axes and an additional scale axis. Therefore, if the scale axis is discretized *appropriately*, different textures will have different signatures at the discretized scales. Denote a wavelet subimage by S (i.e., $a_{(J)}$ and $d^k_{(j)}$ where j=1, 2, …, J and k=h, v, d for a separable 2-D DWT. See also Fig. 1(a)). When a subimage S is treated as a matrix, then the power or energy of the subimage is defined as

$$E_S = \|S\|_F^2 = \sum_{i=1}\sum_{j=1} |s_{ij}|^2 \quad (1)$$

where $\|\cdot\|_F$ and s_{ij} denote the Frobenius norm and (i, j) entry in S, respectively. A feature vector composed of energies of all subimages is also called *wavelet energy signature* [6], one of the most popular wavelet textural features. Entropy and (averaged) l_1-norm of subimages are also frequently used features. Because the normalized energy of each subimage is equal to the variance of a corresponding scale or resolution (for the approximation subimage, mean-centering is needed), the wavelet energy signature represents not only the *presence* of certain signals but also *contrast information* of subimages, when converted to gray scale. Entropy signatures of subimages are equivalent to high-order statistics of wavelet coefficients.

The idea of WTA based on the 2-D DWT can be extended to 2-D wavelet packets (WP) with an arbitrary tree structure [26-28]. When an image is decomposed down to the *J*-th level, the size of a feature vector for an image (when including an approximation subimage) is 3J+1 and 4^J for 2-D DWT and 2-D full-tree WP, respectively. An approximation subimage is sometimes excluded because the variations induced by lighting or illumination are usually captured in the approximation subimage. Based on this idea, several approaches have been proposed. They can be divided into two categories - *filter-oriented* approaches and *feature-oriented* approaches.

2-1. Filter-oriented Approaches

Filter-oriented approaches focus on *optimal* representation of texture through design of filters or the filter bank structure. Although octave-band filter banks (i.e., DWT) generally have good space-frequency tilings for analyzing natural signals, there is no guarantee that the dyadic frequency sampling is always optimal for analyzing texture. Textural features may be most prevalent in intermediate frequency bands [26]. In addition, selection or design of filters may result in substantial performance enhancement since subimages represent *correlations* between localized sections of the raw image and the filters used. Therefore, subimages measure how much the raw image *looks like* the filters. The detailed description of this approach is out of scope of this paper and only brief summary will be given here.

For texture analysis and classification, Chang and Kuo [26] compared the wavelet packet transform with other methods including the DWT, because they discovered that a large class of natural textures can be modeled as quasi-periodic signals whose dominant frequencies are located in the middle frequency channels. The advantage of wavelet packets is the ability to provide a variety of orthonormal bases and corresponding frequency decompositions, from which the *best* one can be chosen. One of the WP decompositions used by Chang and Kuo [26] is shown in Fig. 2(a) and 4-level decomposition of the DWT is shown in Fig. 2(b) for comparison. From these figures, it is clear that the wavelet packet transform provides

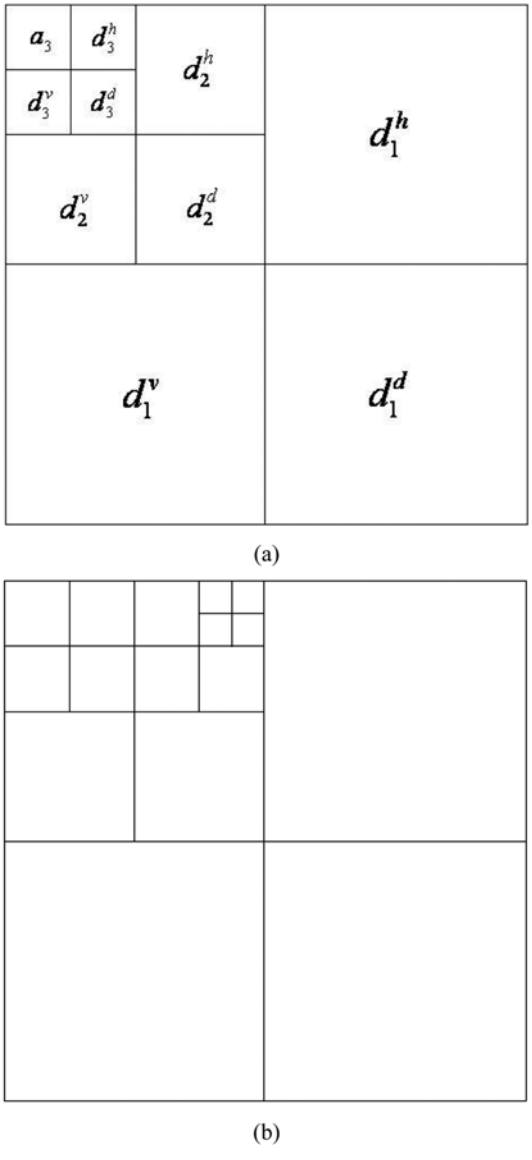

Fig. 2. Two different 2-D wavelet packet tree structures. (a) The standard DWT tree structure down to the third decomposition level. (b) A tree structure used by Chang and Kuo [26]. The subimage in (b), which corresponds to d_2^h in (a), was decomposed further to analyze the middle frequency region ($\pi/4$~$\pi/2$ and 0~$\pi/4$ in vertical and horizontal directions, respectively).

more flexible frequency decomposition than the DWT does.

So far, many multi-channel space-frequency analyses have used banks of filters that are determined regardless of the textures to be analyzed. Although the methods with fixed or heuristically designed filter banks have been reported to produce successful results in several cases, there are also many cases where many of them showed poor performance [4]. In addition, most of these methods produce a large number of features and consequently the follow-up analyses, such as classification and segmentation can be computationally expensive. Hence, filter selection, and even filter design, is gaining interest in many areas involving application of filter banks [4,29]. The design approaches can be categorized according to the following standpoints.

According to applicability, some of the design approaches are restricted to two-texture problems, while others are applicable to multi-texture problems [4]. Also, the type of objective function to be optimized divides the approaches into two categories - optimal representation filters and optimal discrimination filters. Optimal representation filters use the mean-squared prediction error as an objective function to be minimized. This filter design approach can be applied to multi-texture problems. However, being optimal with respect to texture representation doesn't guarantee optimality with respect to the analysis performance. In the optimal discrimination filters, objective functions such as relative feature distance or Fisher's index are used to maximize discrimination power.

2-2. Feature-oriented Approaches

While filter-oriented approaches try to find optimal representation of texture through filter design and simply use energy or entropy as textural features, feature-oriented approaches try to find *good* textural features with fixed filters or the fixed structure of filter bank. Other than common features (i.e., energy and entropy), histogram signatures and co-occurrence signatures were proposed to enhance analysis power [6].

The basic idea of histogram signatures is to capture all first order statistics of a detail wavelet subimage through empirical modeling. It was found experimentally that the detail histograms of natural textures could be modeled by a family of exponentials,

$$h(u)=K\exp(-|u|/\alpha)^{\beta} \tag{2}$$

where the scalar u is an element in the subimage S, K is a normalization factor ensuring $\int h(u)du=1$, β is inversely proportional to the decreasing rate of the peak, and α models the width of the histogram peak [30]. When this model is valid, all first order statistics of detail subimages are completely characterized by two parameters, α and β which are called *wavelet histogram signatures* [6].

In contrast, *wavelet co-occurrence signatures* are direct applications of the work by Haralick et al. [19]. In other words, wavelet co-occurrence signatures are higher order statistics based on co-occurrence matrix of detail subimages [6]. Haralick and his coworkers proposed higher order statistics based on GLCMs for texture analysis since higher order statistics can improve analysis power when first order statistics alone are not enough. Among 14 statistics proposed in [19], the following four statistics are popular ones [4]:

$$\text{Angular Second Moment}=\sum_{i=0}^{G-1}\sum_{j=0}^{G-1}p_{ij}^2 \tag{3}$$

$$\text{Contrast}=\sum_{i=0}^{G-1}N\left(\sum_{|i-j|=n}p_{ij}\right) \tag{4}$$

$$\text{Correlation}=\frac{1}{\sigma_x\sigma_y}\sum_{i=0}^{G-1}\sum_{j=0}^{G-1}ijp_{ij}-\mu_x\mu_y \tag{5}$$

$$\text{Entropy}=\sum_{i=0}^{G-1}\sum_{j=0}^{G-1}p_{ij}\log p_{ij} \tag{6}$$

where G is the number of grey levels, p_{ij} the (i, j) element of a co-occurrence matrix, and μ_x, μ_y, σ_x and σ_y are the means and standard deviations.

Although wavelet energy signature, wavelet entropy signature, and wavelet co-occurrence signatures are statistically well founded, there have been arguments about the performances of energy signatures and entropy signatures [31]. An answer to this issue can be found from Eq. (2). This equation tells us not only that mean values of detail subimages are zero, but also that it can model any symmetric, bell-shaped curve. For wavelet subimages of a texture whose probability distribution functions (PDF) are Gaussian, the mean and the variance are sufficient statistics and the energy signature alone becomes the best representing textural feature. As the PDFs of the detail subimages move away from Gaussian, the energy signature is not the best representing feature anymore but it is still a good feature because the PDF is symmetric. After a certain point, entropy signatures will show better performance than energy signatures and will be the best representing feature when the PDF is sub-Gaussian. This fact can be an answer to the performance issue regarding energy and entropy signatures although the best representing features generally do not guarantee the best classification performance.

AN ILLUSTRATION

In order to illustrate wavelet texture analysis, we used the steel image dataset that was first used by Bharati et al. [15]. This work has attracted enormous attention from many researchers since then and this is one of the reasons for using this dataset in this paper. The same dataset was also used in investigation of (optimal) wavelet packets in texture analysis by the authors [28,32]. The all images in the dataset, image IDs, and corresponding quality evaluations by expert graders are given in Appendix A1. For detailed desriptions of the dataset, please refer to references.

1. Stochastic Nature of a Scene in an Image

As we mentioned earlier, images from process industries exhibit scenes having stochastic nature and this is clear when examining four different images of bad surface quality shown in Fig. 3. Although the four images are all classified as bad quality, they are *not* pixel-by-pixel identical and there is also no pre-determined shape, size, orientation, depth, and a number of pits on the surface (compare this with deterministic scenes from typical manufacturing processes such as printed circuit boards). When analyzing images with stochastic characteristics, a feature space (calculated from the original image space) is preferred to the original image space for this reson, and this is why extracting or calculating features from images is crucial in image texture analysis.

2. Multiresolution Analysis Via Wavelet Transform

While different physical structures in the image are enhanced at

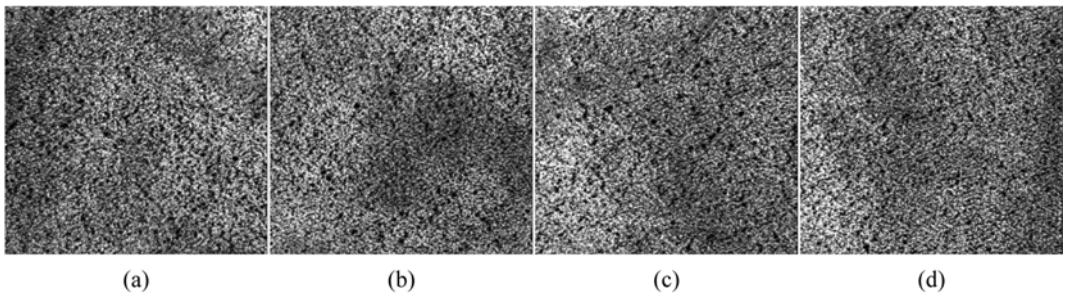

Fig. 3. Examples of four different steel images with the same (Bad) surface quality. Image IDs are: (a) B01, (b) B02, (c) B03, (d) B04.

fine resolution, the larger overall structures that provides the image context are mainly captured at a corse resolution. Multiresolution analysis (MRA) provides a hierarchical framework for identifying (spatial) frequency characteristics of an image in this straightforward manner.

The basic idea of MRA is signal decomposition based upon successive approximations, and thus it is relevant to DWT [30]. Suppose V_0 (=$l_2(Z)$, the space of square-summable sequences) is decomposed into a coarse approximation (a low-pass version) in subspace V_1 and a detail in subspace W_1. The detail signal is the difference between the original signal and its coarse version. Then, this means that the coarse and the detail subspaces are orthogonal to each other

$$V_0=V_1\oplus W_1. \tag{7}$$

Recursive application of this decomposition J times on the coarse approximation yields a sequence of embedded closed spaces

$$V_J\subset\cdots\subset V_2\subset V_1\subset V_0. \tag{8}$$

Then, it is obvious from Eqs. (7) and (8) that

$$\bigcup_{j=0}^{J} V_j = V_0 \tag{9}$$

$$V_0=W_1\oplus W_2\oplus\cdots\oplus W_J\oplus V_J. \tag{10}$$

Realization of this MRA can be done through orthogonal orthogonal discrete wavelet transform (DWT). For further information about MRA, please refer to references [17,30].

To show the usefulness of MRA in image texture analysis, MRA of the image B12 using 4-level DWT with the order-one Coiflet filter is shown in Fig. 4. To accomplish this, horizontal and vertical low-pass filterings *without down-sampling* were performed to the original image (denoted as $\mathbf{a}_0$ in Fig. 4) and its approximation subimages (denoted as $\mathbf{a}_1$, $\mathbf{a}_2$, and $\mathbf{a}_3$ in Fig. 4) at each approximation step. As seen from the axiomatic definition of MRA in Eqs. (7)-(10), the detail subimages are simply differences between two subsequent approximation subimages (i.e., $\mathbf{d}_i=\mathbf{a}_{i-1}-\mathbf{a}_i$ and i=1, 2, 3, 4) due to no down-sampling. Because all elements in wavelet subimages are real numbers, all the subimages were converted to gray-scale images after proper scaling. It is clear from Fig. 4 that the approximation subimage $\mathbf{a}_4$ captures the overall intensity variation across the image, which is mainly ink smudge marks due to manual cleaning of excessive ink [15]. The detail subimage $\mathbf{d}_4$, which corresponds to the lowest spatial frequency, has big dark dots (pits) and the size of pits in the detail subimages becomes progressively smaller as one moves from $\mathbf{d}_4$ to $\mathbf{d}_1$. It can be expected that steel sheets with excellent quality will have more fine pits in the details $\mathbf{d}_1$ and $\mathbf{d}_2$ whereas bad steel surfaces will have more bigger pits in $\mathbf{d}_3$ and $\mathbf{d}_4$.

This will be clear when energy signatures for steel images with different surface qualities are compared to each other. To illustrate this, the same MRA is applied to three steel images with different surface qualities and wavelet energy signatures for the four detail subimages of three images from Fig. A1 are shown in Fig. 5. It is clearly evident that the shift in the distribution from $\mathbf{d}_1$ towards $\mathbf{d}_4$ as one moves from the excellent steel image (E02) to the bad one (B11). In other words, steel images with different surface qualities

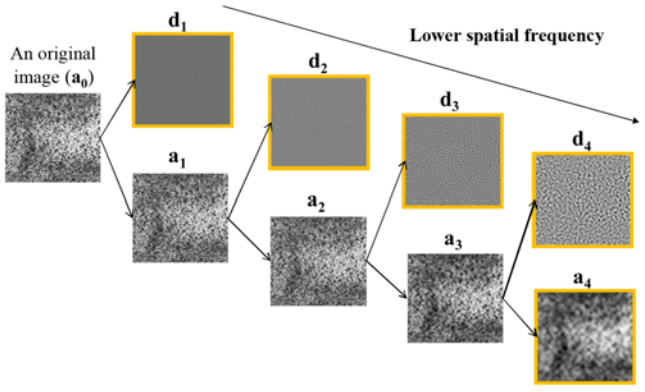

Fig. 4. Multiresolution analysis of a steel image (B12) using 2-D discrete wavelet transform.

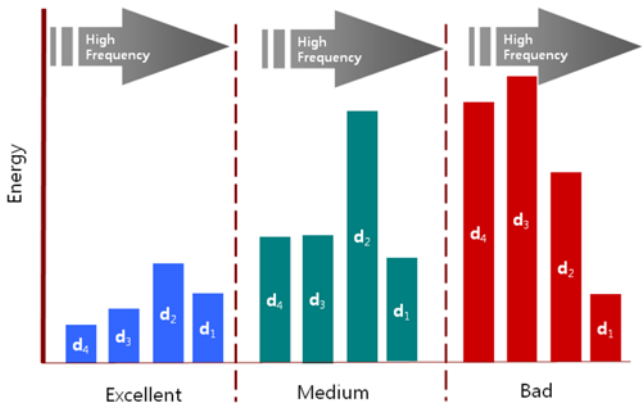

Fig. 5. Wavelet energy signatures of three steel images with different qualities. Image IDs of the three images are E02 (Excellent), M01 (Medium), and B11 (Bad), respectively.

Table 1. Fisher's index values of different wavelet signatures

	Energy	Entropy	l_1-norm
Fisher's index, J	3.12	1.89	3.32

have different wavelet energy signatures and therefore, the basic assumption of WTA is valid for this dataset.

3. Comparison of Different Wavelet Signatures

There are numerous wavelet features used in the literature as mentioned in Section 3.2 and this can pose a problem of choise to researchers or practictioners in process industries. Judging from an authors' experience, the right choice of a feature that will give the best performance solely depends on the very application at hand, i.e., there is *no* such a feature that will work best in every applications. If no prior knowledge about the application under consideration is available, then a trial and error approach is essentially the only method one can resort to. One also needs to keep in mind that the best representing signatures do not necessarily guarantee the best performance.

Seen from the previous MRA results of the steel image dataset, the wavelet energy signature seems to capture characteristics of steel surfaces with different qualities very well and this is why wavelet energy signatures have performed well in the previous studies [15, 28,32]. Performances of three different wavelet signatures - energy, entropy, and l_1-norm signatures - were compared in this section and the results are summarized in Table 1 in terms of Fisher's index, J. A brief summary of Fisher's Discriminant Analysis (FDA) [33] and Fisher's index is given in the Appendix A2.

Since the size of the steel image dataset is relatively small to calculate the index, each original image was divided into four non-overlapping (240×254) smaller images, as shown in Fig. A1 (top left). The new image set, which has a total of 140 images (32 excellent, 36 good, 24 medium, and 48 poor) was used for calculating Fisher's index. The wavelet conditions (decomposition level and the mother wavelet) used were same as in previous section. Seen from Eq. (A2), a better-classifiable signature will have a higher value of Fisher's index among different wavelet signatures and the energy signature have a high value in Table 1 as expected. The entropy signature has the lowest value and the l_1-norm signature has the highest, which is slightly larger than that of the energy signature. The reason for this ($J_{energy} < J_{l_1\text{-}norm}$) could be the robustness of l_1-norm to noise and/or outliers [34], which is also very clear when comparing its formula ($=\sum_{i=1}\sum_{j=1}|s_{ij}|$) with that of the energy signature.

4. Comparison of Different Structures of Wavelet Decomposition

The coefficients of the continuous wavelet transform (CWT), denoted as CWT(a, τ), is defined by the convolution integral

$$\mathrm{CWT}(a,\tau)=\frac{1}{\sqrt{a}}\int f(x)\,\psi\left(\frac{\tau-x}{a}\right)dx \tag{11}$$

where f(x) is a one-dimensinal (1-D) signal, a and τ are continuous scale and shift parameters, respectively. The magnitude of the coefficient is maximized when the frequency of the signal matches that of the corresponding dilated wavelet and therefore, the above equation can be thought as the *correlation* of the input signal f(x) with a time-reversed, shifted, and rescaled version of mother wavelet ψ(x). For this reason, it has been reported that filter design can produce great performance enhancement [4,29] but the majority of related works can be found only in signal processing literature, because filter design requires extensive knowledge in filter bank theory.

On the other hand, the different structures of wavelet decomposition also can affect performance of an analysis and finding the *best basis* has been studied in various fields including Process Systems Engineering [28] and Chemometrics [35,36]. This is because best-basis selection can be done relatively easily through numerical optimization techniques such as branch-and-bound algorithms. To demonstrate the differences in performance of different decomposition structures, four different wavelet decompositions - DWT, full-tree wavelet packets (WP), optimal WP via branch-and-bound algorithms (top-down search), optimal WP via exhautive search (bottom-up search) - were applied to the steel image dataset and results using FDA are summarized in Table 2 and Fig. 6. The same conditions (division of original images, decomposition level, and mother wavelet) were used as in previous section. The *k*-nearest neighbor with k=3 was used in calculating classification error. For each structure, wavelet energy signatures were used to calculate Fisher's index J and this index was employed as an objective function in optimization. The same methodology developed by Kim et al. [28] was used in finding optimal WP. Please refer the reference for detailed information regarding the best-basis selection methods.

It is clear from Table 2 that two optimal WPs (top-down and bottom-up) have very large Fisher's index compared to DWT and it is rather surprising to see that even full-tree WP has lower index than that of the optimal WPs. A wavelet structure with higher Fisher's index will lead to better classification performance and this can be verified in Fig. 6. As one can move from Fig. 6(a) to Fig. 6(d), the between-class distance becomes longer while within-class distance becomes shorter. All classes are completely separated in Fig. 6(c) and Fig. 6(d) and thus they have zero classification error in Table 2, while there are some overlaps between classes in Fig. 6(a) and Fig. 6(b) indicating non-zero classification errors in the table. This is certainly because frequency decomposition of DWT is too coarse to differentiate the space-frequency characteristics of the dataset: when comparing different wavelet structures (DWT in Fig. 2(a) and two optimal WPs in Fig. 7(b) and Fig. 7(c)) with corresponding results (Fisher's index and classification errors), it is clear that certain classes in the dataset have dominant frequencies in some middle frequency regions and thus they cannot be differentiated sufficiently by DWT. For example, top-down search found the WP tree that decomposes only two subimages (corresponding to d_1^h and d_1^d of

Table 2. Comparison of performances using different wavelet decomposition trees

	DWT	Full wavelet packets	Optimal wavelet packet (top-down)	Optimal wavelet packet (bottom-up)
Fisher's index	3.12	8.83	27.94	53.35
Classification errors (%)	4.29	0.71	0	0

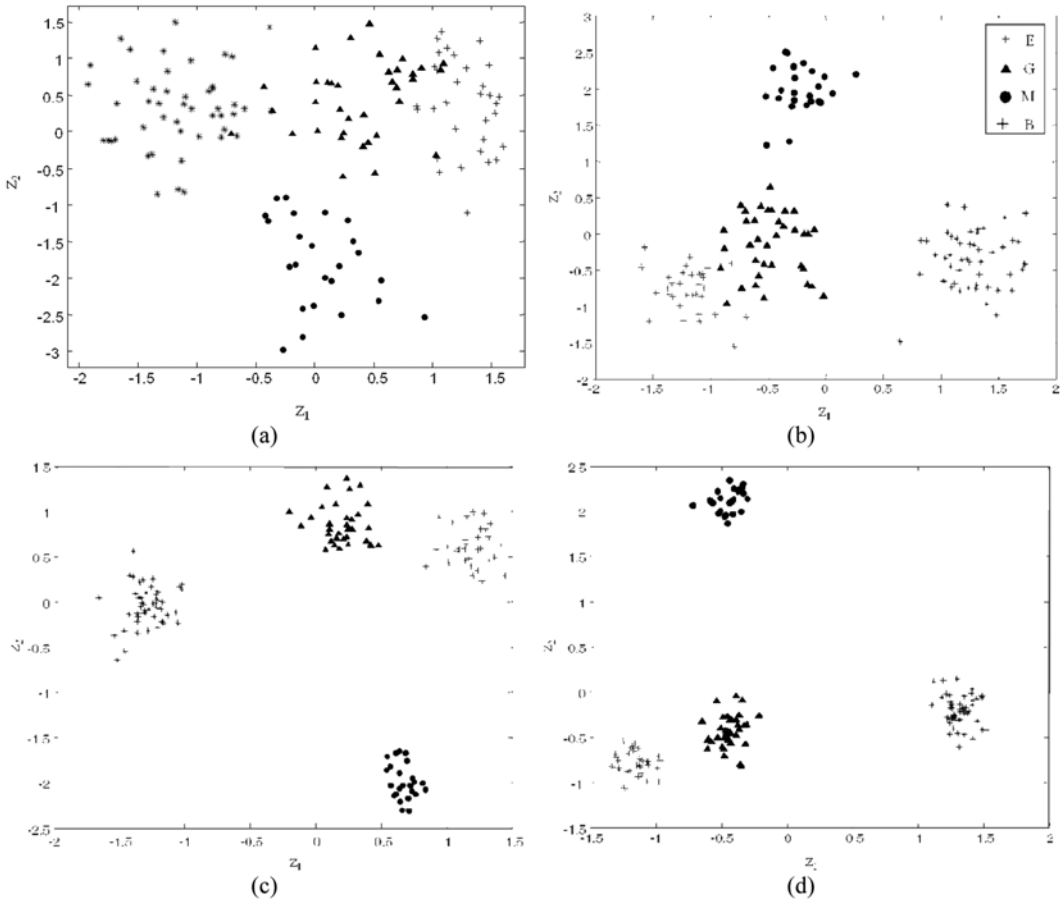

Fig. 6. z_1-z_2 Plots obtained using different structures of wavelet decomposition. (a) DWT, (b) Full WP tree, (c) Optimal WP tree found via top-down search, and (d) Optimal WP tree found via bottom-up search.

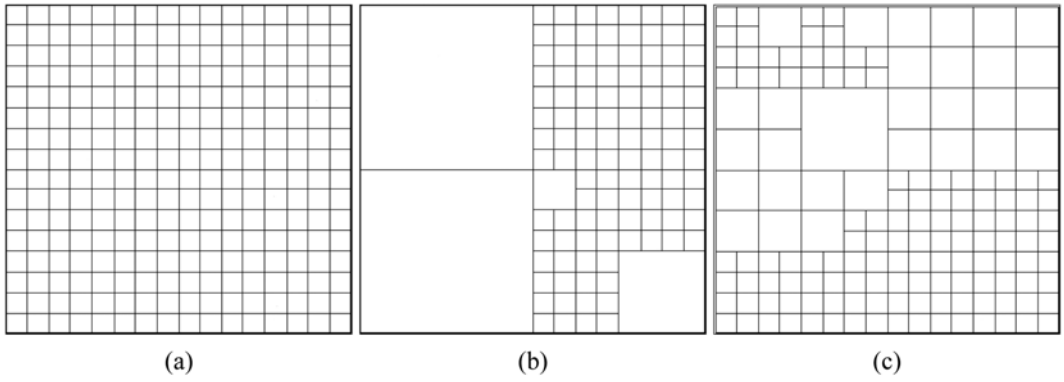

Fig. 7. Different wavelet decomposition structures: (a) Full wavelet packet (WP) tree, (b) Optimal WP tree found via top-down search, and (c) Optimal WP tree found via bottom-up search.

DWT in Fig. 2(a)) further, which have middle and high frequency characteristics, leaving the lowest frequency subimage (corresponding to a_1 in Fig. 1(b)) undecomposed. Full-tree WP is also inadequate because it provides overcomplete orthonormal bases for frequency decomposition, some of which are unnecessary for texture classification. It is clear from Fig. 7(a) and Fig. 7(c) that bottom-up search found the decomposition tree, which is less complicated but provides much larger Fisher index than that of full-tree WP. Another problem is that dimensionality of full-tree WP can deteriorate classification performance.

CONCLUSIONS

In this work, image texture analysis and theories of wavelet texture analysis (WTA) are overviewed and discussed. Important aspects of WTA are also explained and illustrated through classification of

industrial rolled steel sheet samples into various quality grades. Also, the strengths and weaknesses of the different WTA methods become apparent in the discussion of the methodology and in the application to the industrial case study. This can provide researchers and practitioners in process industries with core concepts, ideas and hints regarding WTA and its usage.

WTA methods currently appear to be the most powerful approach to image texture analysis and thus they are excellent candidates for extracting spatial information from images. Especially, the ability to adaptively decompose frequency contents in images and to selectively filter out irrelevant features makes WTA more flexible and powerful.

ACKNOWLEDGEMENT

The authors thank Professor John F. MacGregor at McMaster University for his permission to use the dataset for this study. This work was supported by Basic Science Research Program through the National Research Foundation of Korea (NRF) funded by the Ministry of Education, Science and Tehnology (2010-00003056).

APPENDIX

1. A1 Description of the Dataset

The images in the dataset, image IDs, and corresponding quality

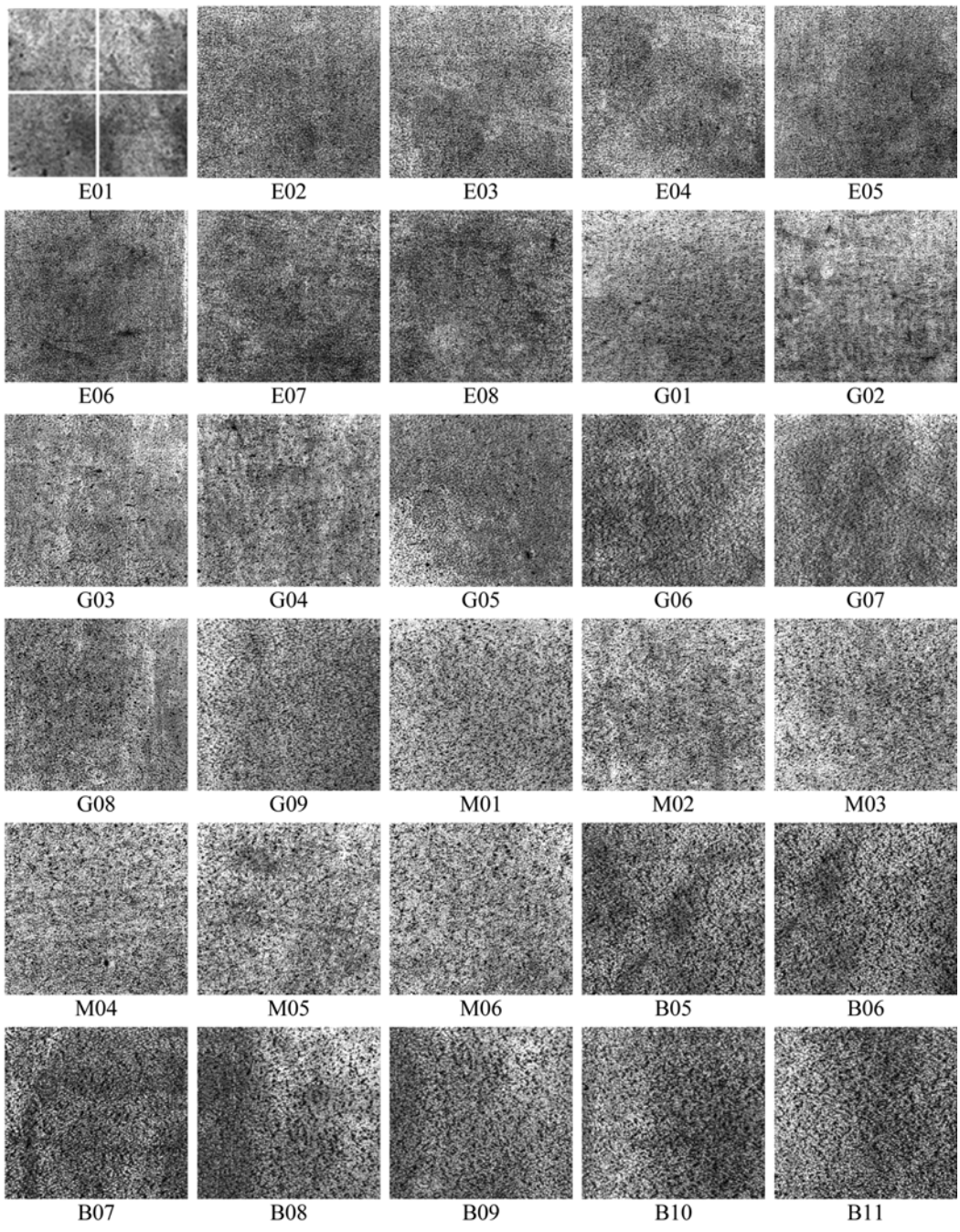

Fig. A1. Steel surface images used in this study.

Table A1. List of 35 images and coresponding expert's evaluations

Image ID	E01	G01	M01	B01
	E02	G02	M02	B02
	E03	G03	M03	B03
	E04	G04	M04	B04
	E05	G05	M05	B05
	E06	G06	M06	B06
	E07	G07		B07
	E08	G08		B08
		G09		B09
				B10
				B11
				B12
Expert's evaluation	Excellent	Good	Medium	Bad

evaluations by expert graders are shown in Fig. A1 and Table A1. (only the images not shown in the main text are shown in Fig. A1.)

2. A2. Fisher's Discriminant Analysis (FDA) and Fisher's Index

Because Fisher's Discriminant Analysis (FDA) is one of supervised learning methods, one needs a class label y as well as the corresponding feature vector **x**. Given *d*-dimensional input data, FDA performs dimensional reduction of the input space onto (*c*-1)-dimensional latent space, where c is the number of classes [33]. Contrary to Principal component analysis (PCA) which finds a latent space representing original data best, FDA finds a latent space that is effective in classification.

We define the between-class covariance matrix $\mathbf{S}_B$ and the within-class covariance matrix $\mathbf{S}_W$ by

$$\mathbf{S}_B = \sum_{i=1}^{c} n_i(\mathbf{m}_i - \mathbf{m})(\mathbf{m}_i - \mathbf{m})^T \tag{A2}$$

$$\mathbf{S}_i = \sum_{\mathbf{x} \in D_i} (\mathbf{x} - \mathbf{m}_i)(\mathbf{x} - \mathbf{m}_i)^T \tag{A3}$$

$$\mathbf{S}_W = \sum_{i=1}^{c} \mathbf{S}_i \tag{A4}$$

where $\mathbf{m}_i$ is the *d*-dimensional sample mean of feature vectors whose label is class i, D_i is a set of all feature vectors from class i, and n_i is the number of feature vectors within D_i, respectively. The mapping matrix **W** maximizes the following

$$J = \frac{|\mathbf{W}\mathbf{S}_B\mathbf{W}^T|}{|\mathbf{W}\mathbf{S}_W\mathbf{W}^T|}. \tag{A5}$$

In other words, **W** minimizes the within-class distance and maximizes the between-class distance when projected. J is called as Fisher's index and it is one of the most popular choices for indirectly indicating classification performance especially when only a finite number of samples are available [37,38]. The projected vector $\mathbf{z}$ ($=\mathbf{W}^T\mathbf{x}$) is also called a discriminant variable.

REFERENCES

1. R. C. Gonzalez and R. E. Woods, *Digital image processing*, Addison-Wesley, Reading (1993).
2. IEEE Standard 610.4. (1990).
3. S. Livens, *Image analysis for material characterization*, Ph.D Thesis, University of Antwerp, Belgium (1998).
4. T. Randen, *Filter and filter bank design for image texture recognition*, Ph.D Thesis, NTNU, Norway (1997).
5. M. Tuceryan and A. K. Jain, in *Handbook of pattern recognition and computer vision*, Texture Analysis. C. H. Chen Eds., World Scientific Publishing, NJ (1998).
6. G. Van De Wouer, *Wavelets for multiscale texture analysis*, Ph.D Thesis, University of Antwerp, Belgium (1998).
7. J. J. Liu, *Machine vision for process industries: Monitoring, control and optimization of visual quality of processes and products*, Ph.D Thesis, McMaster University, Canada (2004).
8. J. J. Liu, J. F. MacGregor, C. Duchesne and G. Bartolacci, *Minerals Engineering*, **18**(1), 65 (2005).
9. J. J. Liu and J. F. MacGregor, *Minerals Engineering*, **21**(9), 642 (2008).
10. J. J. Liu and J. F. MacGregor, *Machine Vision and Applications*, **16**(6), 374 (2006).
11. J. J. Liu and J. F. MacGregor, *Ind. Eng. Chem. Res.*, **44**, 4687 (2005).
12. S. Garcia-Munoz and D. G. Gierer, *Int. J. Pharm.*, **395**, 104 (2010).
13. R. Gosselin, D. Rodrigue and C. Duchesne, *Comput. Chem. Eng.*, In Press (2010).
14. M. S. Reis and A. Bauer, *Chemometrics and Intelligent Laboratory Systems*, **95**, 129 (2009).
15. M. Bharati, J. J. Liu, and J. F. MacGregor, *Chemometrics and Intelligent Laboratory Systems*, **72**(1), 57 (2004).
16. A. Materka and M. Strzelecki, *COST B11 Report*, Technical University of Lodz, Institute of Electronics, Brussels (1998).
17. M. Vetterli and J. Kovacevic, *Wavelets and subband coding*, Prentice Hall, Englewood Cliffs (1995).
18. B. Julesz, *Scientific American*, **232**(4), 34 (1975).
19. R. M. Haralick, K. Shanmugam and I. Dinstein, *IEEE Transactions on Systems, Man, and Cybernetics*, **3**, 610 (1973).
20. D. C. He and L. Wang, *Pattern Recognition*, **25**, 391 (1991).
21. C. Sun and W. G. Wee, *Computer Vision, Graphics, and Image Processing*, **23**, 341 (1983).
22. M. D. Levine, *Vision in man and machine*, McGraw-Hill Inc., New York (1985).
23. G. Cross and A. Jain, *IEEE Transactions on Pattern Analysis and Machine Intelligence*, **5**, 25 (1983).
24. J. M. Keller, S. Chen and R. M. Crownover, *Computer Vision, Graphics, and Image Processing*, **45**, 150 (1989).
25. J. G. Daugman, in *Computational Neuroscience*, E. L. Schwartz Ed., MIT Press, Cambridge (1988).
26. T. Chang and C. C. J. Kuo, *IEEE Transactions on Image Processing*, **2**, 429 (1993).
27. K. Etdmad and R. Chellappa, *IEEE Transactions on Image Processing*, **7**, 1453 (1998).
28. D. Kim, C. Han and J. J. Liu, *Ind. Eng. Chem. Res.*, **48**(5), 2590 (2009).
29. Y. Mallet, D. Coomans, J. Kautsky and O. De Vel, *IEEE Transactions on Pattern Analysis and Machine Intelligence*, **19**, 1058 (1997).
30. S. G. Mallat, *IEEE Transactions on Pattern Analysis and Machine Intelligence*, **11**, 674 (1989).
31. A. Laine and J. Fan, *IEEE Transactions on Pattern Analysis and Machine Intelligence*, **15**, 1186 (1995).

32. J. J. Liu, D. Kim and C. Han, *Ind. Eng. Chem. Res.*, **46**(15), 5152 (2007).
33. R. A. Fisher, *Annals of Eugenics*, **7**(Part II), 179 (1936).
34. N. Kwak, *IEEE Transactions on Pattern Analysis and Machine Intelligence*, **30**(9), 1672 (2008).
35. M. Cocchi, R. Seeber and A. Ulrici, *Chemometrics and Intelligent Laboratory Systems*, **57**(2), 97 (2001).
36. B. Walczak and D. L. Massart, *Chemometrics and Intelligent Laboratory Systems*, **38**(1), 39 (1997).
37. A. Biem, S. Katagiri and B. H. Juang, *IEEE Transaction on Signal Processing*, **45**, 500 (1997).
38. R. P. W. Duin and R. H. Umbach, *IEEE Transaction on Pattern Analysis and Machine Intelligence*, **23**, 762 (2001).